Interpretation of the pressuremeter test into clay in unsaturated and undrained condition

Jacques Monnet [1], *Luc* Boutonnier[2]

[1]*Gaiatech , 22 rue Antoine Chollier, Seyssinet F-38170, France ;*
[2]*Egis Geotechnique, 3 rue Docteur Schweitzer, 38180, Seyssins, France*

ABSTRACT

The pressuremeter measures both the pressuremeter modulus and the limit pressure, which are used to estimate the bearing capacity of the foundation according to different standards. The results of the pressuremeter test include the pLM limit pressure and the EM pressuremeter modulus. These quantities cannot be directly input as data for geotechnical calculations using Finite Elements or Finite Differences in the study of civil engineering structures such as retaining walls, tunnels, embankments, and excavations. These modern calculation methods require, at a minimum, knowledge of the mechanical characteristics of the soil, including elasticity (with Young's modulus (E) and the Poisson ratio (ν)) and resistance (with cohesion (c') and the angle of friction (Φ')). This study is devoted to the interpretation of the pressuremeter test so that it is possible to use it for the determination of the mechanical characteristics of the soil. When the pressuremeter test is carried out into clay, it appears pore pressure during the test when only shearing is applied. In summary, understanding pore pressure and interpreting measurements to determine the effective shear modulus are crucial for geotechnical engineering and subsurface exploration. Effective shear modulus can differ significantly from the value determined solely based on total pressure. This study provides the theoretical value of the Skempton coefficient B. Additionally, it proposes an interpretation theory for the pressuremeter test in clay. Finally, the theory is validated through a comparison with tests performed in London clay at a depth of 20.6 meters

Keywords: pressuremeter; interpretation; unsaturated; undrained

1. Introduction

In fine soils, pressuremeter tests are most often undrained and interpreted as total stress (Carter et al. 1979), (Monnet and Chemaa 1994), (Cao et al. 2001). Considering the test in total stress does not achieve the fundamental mechanical characteristics of the soil, as the effect of suction or pore pressure is integrated into the mechanical behaviour to represent the test. In addition, in the numerical tools available to engineers today, theoretical models more sophisticated than Mohr Coulomb's elastoplasticity are available, which allow to consider all or part of the following behaviour of soils for the most common calculation codes (Flac; Plaxis; ZSoil; etc...):

- Hardening Soil Model (HSM, Plaxis., 2021), virgin shear modulus decreases with increasing strain
- Hardening Soil model with SMALL strain stiffness : decreasing shear modulus on unloading-reloading with increasing shear strain (HS Small; Plaxis , 2021)

Within these models, multiple modules exist, each varying based on the applied load. In this study, one of the objectives is to conduct a finely interpreted pressuremeter test with loading cycles. Additionally, we propose considering pore pressure and effective stresses for a quasi-saturated undrained soil.. The notion of Quasi-Saturated soil corresponds to the fact that there is very often, even in soils below the water table, a part of air which is present in the form of occluded bubbles inside the solid skeleton (Boutonnier 2007). The compressibility of this occluded water-air mixture leads to a partial transfer of the total isotropic stresses to the skeleton. In the interpretation of the pressuremeter, these phenomena must be considered. This paper is based on theoretical developments validated on a pressuremeter test in London clay. Starting from a previous study (Monnet et al. 2021) we develop the current model, by taking into account the nonlinear elasticity, which explains the pore pressure build-up (whereas the linear elasticity model does not allow an increase in pore pressure during shearing). Finally, we solve the plastic behaviour with a Mohr-Coulomb plasticity. This paper lays down the principles of theoretical development, the main results, and the practical conclusions that can be drawn.

2. State of the art

Many studies have been devoted to the interpretation of the pressuremeter test in clays. The main studies were carried out with different assumptions:

- Study under total stress, i.e. without separating the role of pore water from that of the solid skeleton as for (Gibson and Anderson 1961) (Wroth and Windle 1977) (Monnet and Chemaa 1994) (Arulrajah et al. 2011) (Habert and Burlon 2020). In this research axis, when the permeability is too low, it becomes challenging to determine the state of effective stresses. Additionally, the evolution of total orthoradial stresses exhibits

symmetry with the total radial stress originating from p_0, which is not accurate.

- Behaviour under total stress, but with a plastic limit given by the Cam Clay model without explaining the origin of the increase in pore pressure, nor the evolution of the shear modulus G'. This is the case for several numerical studies (Carter et al. 1979) (Silvestri and Abou-Samra 2012). These models do not predict an increase in pore pressure as a function of shear as observed, but only as a function of the effective isotropic pressure, which does not vary along shearing.

.- Total stress behaviour that links the total pressure at the drilling to its deformation by a power law (Hughes and Whittle 2023); This last solution does not allow us to know the effective stress state, nor the state of deformation at any point in the radius around the pressuremeter gauge

- Hypothesis of a Quasi-Saturated, Undrained soil; initially assuming linear elastic soil behaviour (Monnet et al. 2021). This first step shows no generation of pore pressure in a linear elastic soil. So in this study we assume a distortion-dependent shear modulus based on previous work (Santos and Correia 2001), mostly used in soil mechanics numerical software.

3. Theoretical basis of development

3.1. Different states of saturation

Many authors have mentioned the existence of 4 saturation domains, each with a distinct behaviour. This hypothesis is taken up in the design of our model based mainly on previous work (Boutonnier 2007). The behaviour of an unsaturated soil can be classified into 5 domains depending on the degree of saturation.

Domain D0-Adsorption: $s \geq s_{air}$ and $S_r \leq S_{rres}$

The soil is practically dry; all that remains is the water adsorbed around the solid particles; The suction is higher than the $s_{air\ inlet}$ suction; the degree of saturation S_r is lower than the degree of saturation related to the S_{rres} adsorption regime

Domain D1: Unsaturation $s \geq s_{air}$ and $Sr \leq S_{rair}$:

The gas phase is continuous in the soil sample under consideration. This state corresponds to a suction s greater than the inlet suction of $s_{air\ inlet}$ and a degree of saturation lower then the degree of saturation related to the air entry state.

Domain D2: Occluded Air with succion

$s \leq s_{air}$ and $S_{rair} \leq S_r \leq S_{re}$:

In this area, the open air has disappeared. The air is occluded in the sample under consideration. Suction has the effect of increasing the intergranular contact forces.

Domain D3: Occluded Air with pore pressure

$S_{re} < S_r < 1$ and $u_w > u_{we}$:

Air is occluded into the soil sample in the form of air bubbles that are virtually independent of the skeleton. The capillary suction, which exists on the surface of each bubble, has no effect on the contact forces between soil grains at the macroscopic scale. Here we can consider that D3 corresponds to the case of positive pore pressures with $S_r < 1$, which is equivalent to use the assumption $u_{we} = 0$

Domain D4: Saturation Sr = 1 :

There is no gaseous air in the soil sample. The soil is perfectly saturated. The boundary between D3 and D4 can also be expressed through the pore pressure u_{wsat} for which $S_r = 1$.

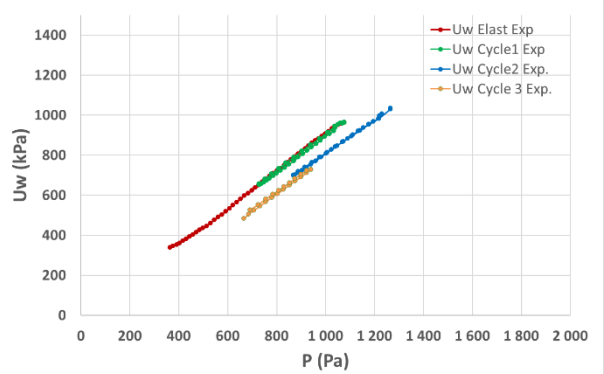

Figure 1: Elastic behaviour - Determination of B_{pres}=0.925 on virgin loading and 3 cycles

3.2. Elastic Undrained behaviour of the soil

A relationship analogous to the relation of (Skempton 1954) can be observed experimentally in elasticity (Figure 1) for the pressuremeter carried out in London clay, fast enough to be considered to be in Undrained condition. In the pressuremeter test, the radial stress is the major stress, the orthoradial stress is the minor. Considering a circular area (Figure 2) between the Ri and Ri-1 radius. This circular area is of cross-section S (1) and deforms under the action of the pressure during drilling and its variation is then dS. Noting that dRi is the displacement ui and dRi-1 is the displacement ui-1, the equation allows determination of the change in volume and the pore pressure by (2) and (3). Please note that (3) is the theoretical expression of the Skempton Bpres coefficient adapted to the pressuremeter In the test presented (Figure 1), we measure an average value of $B_{pres} = 0.925$; in accordance with equation (3) and the measured values of c_f, n and G'_s. The relation between Total and Effective stress can also be obtained (4)

$$S = 2.\pi.(R_{i-1}^2 - R_i^2) \quad (1)$$

$$\delta u_{wi} = -\delta\varepsilon_v / c_f.n = \delta\sigma'_{ri} / c_f.n.G'_s \quad (2)$$

$$\delta u_{wi}/\delta\sigma_r = 1/(1 + c_f.n.G'_s) = B_{pres} \quad (3)$$

$$\delta\sigma'_r = \delta\sigma_r\ (1 - B_{pres}) \quad (4)$$

3.3. Elastic behaviour of the solid skeleton

The previous model (Santos and Correia 2001) provides a way to account for shear modulus dependency on shear strain, which is crucial for capturing pore pressure effects. It is also used in Plaxis as HSM Small (Plaxis corp. 2021). Furthermore, the evolution of the shear secant modulus of the model fits our experimental data (**Figure 7**).

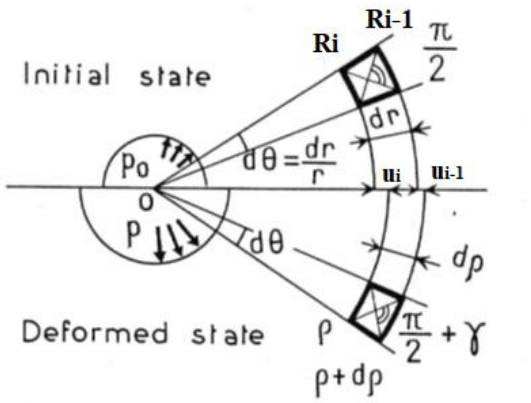

Figure 2: Equilibrium and deformation of the elementary prism in the horizontal plane from (Baguelin et al. 1978)

For the elastic virgin loading, we use the Isotropic Hardening models of (Plaxis corp., 2021), for which the shear-strain relationship is a branch of hyperbola (Duncan and Chang 1970). The equilibrium of the elementary prism (5), is revised by the linear relation between Total and Effective stress (4) with a coefficient B_{press} constant. It becomes (6) which gives us the distribution along the radius of the Total Stress σ (7), of the Effective Radial Stress σ' (8), and the Effective orthoradial Stress σ_θ' (9). Assuming (Skempton 1954) hypothesis, the theoretical solutions (7) (8) (4) are independent of G'.

$$r.d\sigma_r/dr + \sigma_r - \sigma_\theta = 0 \quad (5)$$

$$r.d\sigma'_r/dr + r.du_w/dr + \sigma'_r - \sigma'_\theta = 0 \quad (6)$$

$$\sigma_r = a^2/r^2 . (p - p_0) + p_0 \quad (7)$$

$$\sigma'_r = a^2/r^2 . (p' - p'_0) + p'_0 \quad (8)$$

$$\sigma'_\theta = a^2/r^2 . (p'_0 - p') + p'_0 \quad (9)$$

3.4. Plastic behaviour of the solid skeleton

For plastic behaviour, we use a Mohr-Coulomb plastic analysis, with a cohesion c' and a friction angle Φ' (10), which gives the Frictional Ratio N_f (11); the plastic deformation is ruled by the dilatancy Ψ, which gives the Plastic Ratio n_e (12). The equilibrium of the elementary prism in Effective Stress is given by (6). Noting the relationship between radial and orthoradial effective stresses by (10) as well as the relationship between strains (12), the equilibrium equation transforms into the equation (13)

$$f(\sigma) = \sigma'_r - \sigma'_\theta - sin\Phi'.(\sigma'_r + \sigma'_\theta) - 2.c'.cos\Phi' = 0 \quad (10)$$

$$N_f = (1 - sin\Phi')/(1 + sin\Phi') \quad (11)$$

$$n_e = -(1 - sin\psi)/(1 + sin\psi) = -d\varepsilon_r^p/d\varepsilon_\theta^p \quad (12)$$

$$Ln\left(\frac{p' + c'/tg\Phi'}{\sigma'_{rb} + c'/tg\Phi'}\right) = \left(1 - B_{pres}^p\right).\left(1.-N_f\right)/(1 + n_e).Ln(\varepsilon_{\theta a}/\varepsilon_{\theta b}) \quad (13)$$

The slope γ of the Log-Log relation (13) between the corrected Effective Stress at the borehole p' and the Orthoradial strain at the borehole $\varepsilon_{\theta a}$ is equal to (14). This linear relation can be observed in London clay (**Figure 4**). This slope is analogous to the slope δ of relation (29) of (Monnet 2012) for which c'/TgΦ' has been added to the stress state and the strain state is corrected by $\left(1 - B_{pres}^p\right)$.

$$\gamma = \left(1 - B_{pres}^p\right).\left(\mathbf{1}.-N_f\right)/(1 + \boldsymbol{n_e}) \quad (14)$$

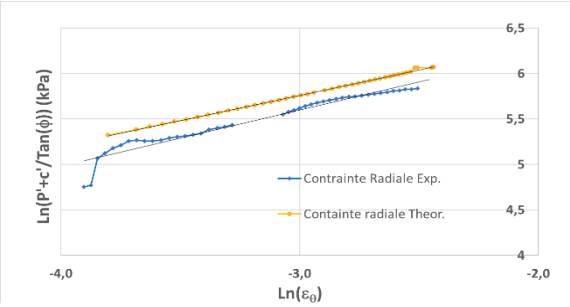

Figure 3 : Evolution of the Effective pressure as a function of the ortho-radial strain - London Clay at 20.6m

The plastic radius b separates the plastic area close to the borehole to the elastic area farther. The equilibrium at this radius b can be considered as elastic but also plastic with the Mohr-Coulomb criterion. It allows determining the effective radial $\boldsymbol{\sigma'_{rb}}$ (15) the orthoradial stresses $\boldsymbol{\sigma'_{\theta b}}$ (16) the pore pressure $\boldsymbol{u_{wb}}$ (17) and the orthoradial strain $\boldsymbol{\varepsilon_{\theta b}}$ at radius b (18).

$$\sigma'_{rb} = p'_0.(1 + sin\Phi') + c'.cos\Phi' \quad (15)$$

$$\sigma'_{\theta b} = \sigma'_r.N_f - 2.c'.cos\Phi'/(1 + sin\Phi') \quad (16)$$

$$u_{wb} = B_{pres}.(\sigma_{rb} - p_0) + u_{w0} \quad (17)$$

$$\varepsilon_{\theta b} = (p'_0.sin\Phi' + c')/(2.G'_{sB}) = -\varepsilon_{rb} \quad (18)$$

3.5. Behaviour of the air-water mixture – c_f

To simplify the theoretical calculations, the behaviour of the interstitial fluid is assumed with a constant coefficient of compressibility of the fluid c_f. The product cf.n is a common factor in pore pressure. As the value of the creep pressure is known (15), the different values of stress and strain can be measured at the plastic radius b. The value of the product cf.n can be deducted from (19). Assuming n=0.4 for this clay, we deduce c_f=1.66.10^{-4} kPa^{-1} which corresponds to a domain D3 - Occluded air with pore pressure, the compressibility of the water alone being c_w=4.2.10^{-7} kPa^{-1}

$$c_f.n = \left(1/B_{pres} - 1\right)/G'_{sb} \quad (19)$$

3.6. Plasticity - Undrained behavior

Starting from (12), the following equations can be deduced (20) (21) (22). The relation (21) gives the slope β of the linear relation between pore pressure and orthoradial strain. The pore pressure increases in the plastic phase as observed (**Figure 4**). On the other hand, the slope β (21) of the linear relationship between u_w and ε_θ allows us to determine the dilatancy Ψ by (22), which is negative and indicates a contraction. In the case of the London clay, the contraction is equal to -3.7°.

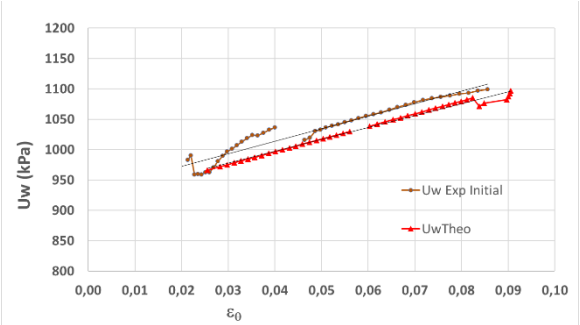

Figure 4: Plastic behaviour - Experiment & Theory: Evolution of effective pressure as a function of orthoradial deformation

The slope of the linear relation between the pore pressure and the Total pressure (**Figure 5**) can also be calculated by (23) and (24) and corresponds to the experimental value $B^p_{pres} = 0.4$

$$\delta\varepsilon_v = 2.sin\psi/(1+sin\psi).\delta\varepsilon^p_\theta \quad (20)$$

$$\delta u^p_w = -2sin\psi/\left[(1+sin\psi)c_f n\right]\delta\varepsilon^p_\theta = \beta.\delta\varepsilon^p_\theta \quad (21)$$

$$sin\psi. = -\left(\beta.c_f.n\right)/\left(2+\beta.c_f.n\right) < 0 \quad (22)$$

$$\delta u_w = B^p_{pres}.\delta\sigma_r = B^p_{pres}/\left(1-B^p_{pres}\right).\delta\sigma'_r = -2.sin\psi/\left[(1+sin\psi).c_f.n\right].\delta\varepsilon^p_\theta \quad (23)$$

$$B^p_{pres}. = -sin\psi/\left[(1+sin\psi).c_f.n.G'_s - sin\psi\right] \quad (24)$$

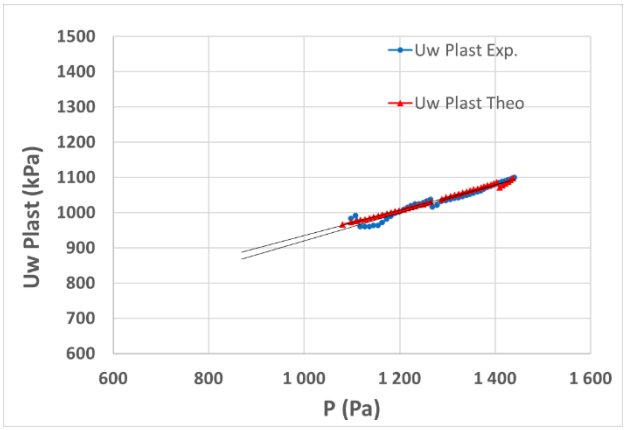

Figure 5: Plastic behaviour Experiment & Theory - Evolution of pore pressure as a function of Total pressure in plasticity drilling - determination of B_{ppres}=0.40

4. Experimental measurements – validation of the theoretical model

The pressuremeter test was performed with a Camkomer probe of 88mm diameter at 20.6m in London clay. The drilling was carried out in self-drilling, with mud pressure to raise the cuttings. Total stress, pore pressure and strain at the borehole were measured.

4.1. Initial state – plastic threshold

The initial state is reached at the intersection between the linear evolution of the pore pressure at the beginning of the test (below p_0=373kPa, **Figure 6**) and the linear relation in the elastic state (up p_0=373kPa, **, Figure 6**). The values of p_0=373kPa and u_{w0}=328kPa correspond to this state. It should be noted that for the pressuremeter test carried out in the London clay at a depth of 20.6m, the Total vertical stress is estimated at 412kPa, and as the water table is 3m depth the initial pore water should be 176kPa. The difference between the theoretical pore water and the measured one is considered to be the effect of the mud pressure used to remove the cutting from the borehole.

The plastic threshold is determined by the intersection between the linear elastic relation between the pore pressure and the total pressure (below p_f= 1050kPa, **Figure 6**) and the linear plastic behaviour between the pore pressure and the total pressure (up p_f= 1050kPa, u_{wf}=951kPa **, Figure 6**).

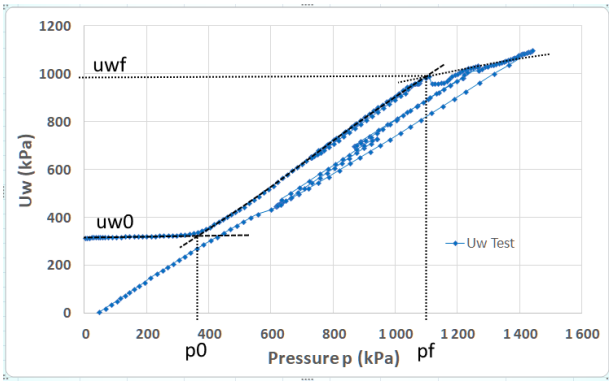

Figure 6: Experiment - Evolution of pore pressures vsersus p during the test –initial state : determination of p_0=373kPa and u_{w0}=328kPa -plastic threshold p_f=1050kPa and u_{wf}=951kPa

4.2. Effective shear modulus at cyclic loading

The cyclic behavior is governed by the HSsmall model (Plaxis Corp., 2021). The determination of the parameters is achieved by calibrating the secant shear modulus with respect to distortion (**Figure 7**) and by controlling the theoretical behavior to match the experimental behavior in the relationship between total pressure and deformation during cycles (**Figure 8**) The parameters are shown (Table 1). The shear moduli are shown (Table 2). We do observe a theoretical hyteresis loop that corresponds to the experiment, over the three cycles in the pressure-strain relationship. When the cut-off deformation $\varepsilon_{\theta cut\text{-}off}$ (model HSsmall, Plaxis corp., 2021) is reached, the tangent shear modulus G'_{tsu} is constant (Table 1).

Table 1. Parameters used in numerical validation of Test

Param.	Variable	Value
e_0	Initial void ratio	0.667
σ_z	Vertical stress	458 kPa
p_0	Horizontal stress at rest	376 kPa
p'_0	Eff. horizontal stress at rest	45 kPa
c'	Eff. cohesion	37 kPa
Φ'	Eff. friction angle	22°
Ψ	Eff. dilatancy	-3.7°
G'^{Ref}_0	Eff. Init. Shear modulus	30000 kPa
G'_{50}	Eff. Shear modulus at 50% resist.	6000 kPa
G'_{tsu}	Eff. Tang. Shear modulus at large deformation	6000 kPa
$\varepsilon_{\theta L}$	Circumf.strain at G_s=0.722.G_0	.00037
$\varepsilon_{\theta b}$	Circumf. Srain at radius b	0.022
ν	Poisson ratio	0.2
c_f	Compres. Coef. air+water	1.66E-04
R_f	Failure ratio	0.900
B_{Pres}	Skemoyon Coef. For Pres.	0.925
C_γ	Coefficient of slope	4.4
P_{Ref}	Reference presssure	100 kPa
u_{wo}	Initial pore pressure	328 kPa

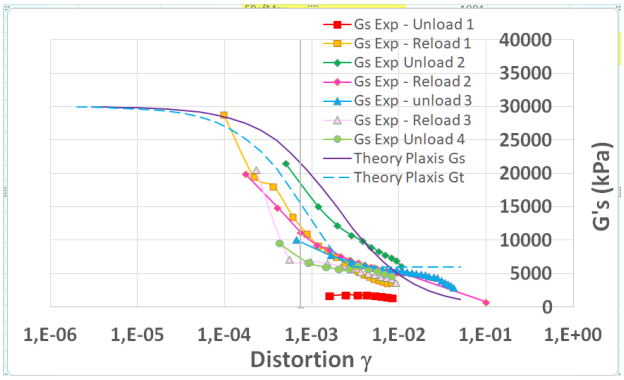

Figure 7 : Evolution of the drained and secant shear modulus during the test – determination of G'^{Ref}_0 = 50000kPa G'_{Stat} = 2000kPa G'_{50}=6000kPa and $\varepsilon_{\theta L}$ =4.10^{-4}; p^{Ref}=100kPa

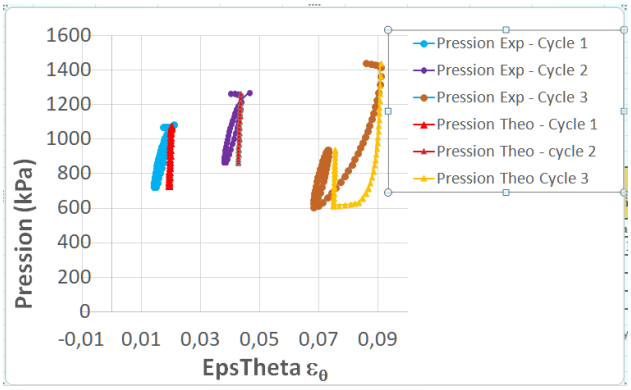

Figure 8 : Experiment-Theory: Control of the cyclic behaviour model. on cycles 1 to 3 of the London clay test – Total pressure, strain relationship.

4.3. Shear characteristics and plasticity

Plasticity is defined by 4 parameters (c'; Φ'; Ψ; Cγ) First, the creep pressure is determined by the change in slope of the uw-p relationship (Figure 6). This change is obtained for our test at u_{wf}=951kPa, p_f=1050kPa, p'_f=99.5kPa, and $\varepsilon_{\theta b}$=0.02226. As the theoretical expression of p'_f is known by (15) , it allows us to find several pairs of possible values (c'; Φ') as well as $\varepsilon_{\theta b}$ (18) which allows determining G'_{sb}=1357kPa. Here, we have chosen the average value (c'=37kPa; Φ'=22°)

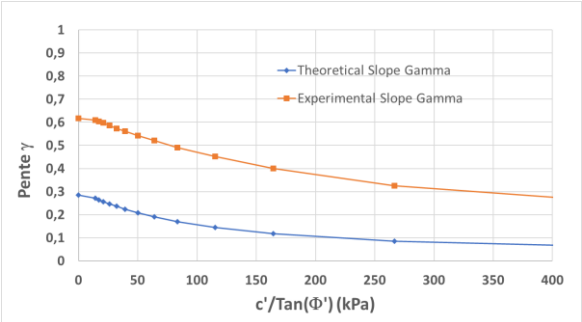

Figure 9 : Comparison of Theoretical and Experimental Slopes of the Log-Log Linear Relationship Effective Pressure and Strain

The different theoretical slopes of this relationship have been tested and a slope that is lower than the experimental slope has been found. The theoretical and experimental slopes as a function of c'/tanΦ' have been plotted (Figure 9). Since we have neglected the time dependant phenomenon as the pressure varies (see uw Exp.-Figure 13, the distortion increases ε_θ=0.085-0.090 when the pore pressure decreases between u_w=1099-895kPa) we introduce a slope correction coefficient Cγ (25). Its value is fixed by the average value of the ratio between the two types of slopes (Figure 9) equal to 4.4.

$$\gamma = \left(1 - B^{p}_{pres}\right).\left(\mathbf{1}.-N_f\right)/(1+\boldsymbol{n_e}).C_\gamma \qquad (25)$$

4.4. Behaviour of the mixture air-water

In elasticity, we use the relation of (Skempton 1954) applied to the pressuremeter (3), which allows us to determine by the mean slope (Figure 1) a single value of B_{pres}=0.925 .

In the context of plasticity, the increase in pore pressure is associated with the contractancy (Ψ). This contractancy is determined by the slope of the relationship between the pore water pressure (u_w) and the orthoradial strain (ε_θ), as depicted in **Figure 5**. Notably, a contractancy value of -3.7° has been identified.

4.5. Virgin loading – Shear modulus difference calculated from Total Pressure or Effective Pressure

For a linear elastic soil, the shear modulus does not depend on pore pressure and there is equality between the drained and undrained modulus. This assumption is contradicted by the measurements carried out. The shear parameters on virgin loading obtained by the different usual methods are compared (Table 2); It can be seen that the shear modulus, measured at virgin loading, is much stronger (Table 2, col.2, lin. 2) calculated in Total Stress than the one calculated in Effective Stress in a ratio of 20 (Table 2, col.4, lin. 2).

4.6. Cyclic loading – Shear modulus difference calculated from Total Pressure or calculated from Effective Pressure

The values of the mean shearing elastic moduli measured with Total Stress or with Effective Stress have been calculated over the three cycles (Table 2). The shearing elastic modulus during the cycle is significantly higher under Total Stress conditions (as shown in Table 2, column 10, lines 3-6) compared to the value calculated under Effective Stress conditions. The ratio between these two moduli is 8 (Table 2, column 5, lines 3-6).

4.7. Verification against the evolution of stresses along the radius

Considering the strains (**Figure 10**), there is complete symmetry of the deformations in elasticity (for radii larger than b=0.092m) and almost complete symmetry in plasticity related to soil contractancy (for radii smaller than b=0.092m).

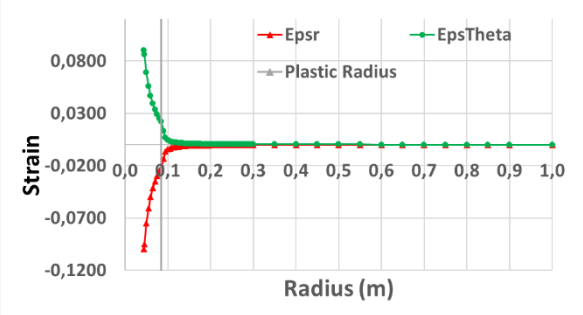

Figure 10 : Nonlinear Elasto-plasticity Solution - Evolution of deformations in clay – applied pressure 1440kPa

Considering the total stresses (Figure 11) there is no symmetry of the stresses with respect to p_0, given the influence of the pore pressure on the radial and orthoradial stresses. Note that the pore pressure gives the general appearance of the total stress curves.

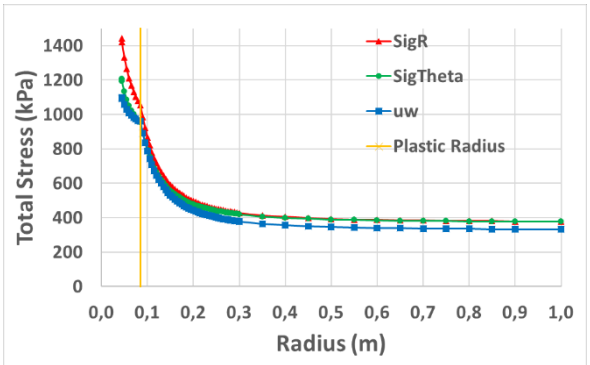

Figure 11 : Nonlinear Elasto-plasticity Solution - Evolution of Total stress in clay – applied pressure 1440kPa

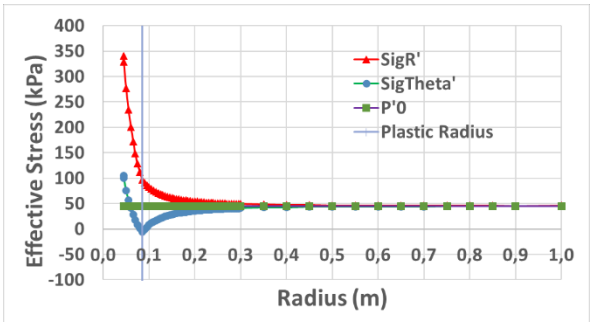

Figure 12 : Nonlinear Elasto-plasticity Solution - Evolution of Effective stress in clay – applied pressure 1440kPa

Considering the evolution of the effective stresses (Figure 12), for the elasticity part (part of the curves to the right of the plastic radius b=0.092m), the effective stresses are symmetrical with respect to p'0; the radial effective stress defines the stress level; the orthoradial effective stress σ'_θ is symmetric to σ'_r with respect to p'0. For the plastic part (part of the curves to the left of the plastic radius b=0.092m), the effective stress is imposed by the loading condition at the borehole, and the orthoradial stress follow the radial stress depending on the Mohr-Coulomb criteria.

4.8. Verification against the relation Total Pressure – Deformation at the borehole

4.8.1. Elastic behaviour (virgin loading, for p<1050kPa and cycles)

On the virgin loading (Figure 13), the theoretical curve (Sr Teo, Red triangle) recovers the experiment curve (Sr Exp, Purple circle) with a slightest higher curvature; on the three cycles, the theoretical slope of cycles is higher than the experimental one, linked to a smaller value of Bpres coefficient. As we assume in this simplified theory a value of Bpress constant, it is not yet possible to find a better correspondence between theory and experiment on cycles.

Table 2. Experimental shear parameters for the pressuremeter used (kPa)

Variable	G_s Virgin	G_s Cyclic	G'_s Virgin	G'_s Cyclic	G'_{ss0}	G'_{s50}	G'_{sFin}	G_s/G'_s	G_s Cycl/Gs-Virgin
Virgin-Load	14023		706		10904	7162	706	19.9	1.9
Cycle 1		25629		3001	20000		3001	8.5	4.3
Cycle 2		23350		3504	20000		3504	6.7	5.0
Cycle 3		29976		3998	20000		3998	7.5	5.7

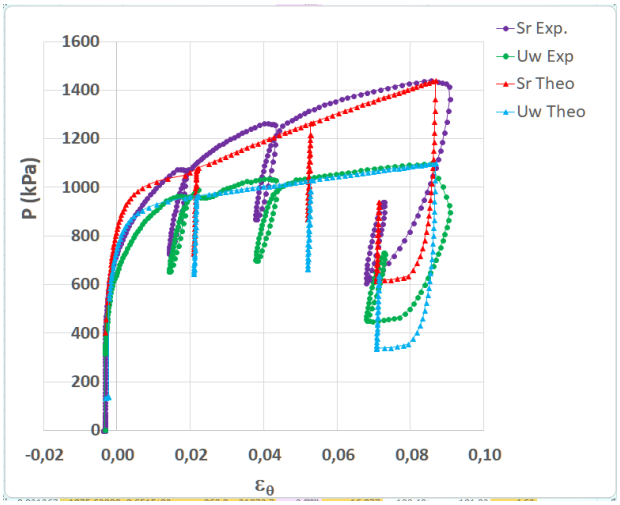

Figure 13 : Validation of the theoretical results on pressuremeter test in London clay at 20.6m depth, . Φ=22°, c'=37Pa, Ψ=-3.7°

.

4.8.2. Plastic behaviour (virgin loading, for p>1050kPa

On the plastic behaviour (Figure 13), the evolution of the theoretical pressure (Sr Teo, Red triangle) recovers the experiment curve (Sr Exp, Purple circle) quite well, the maximum deformation being the same.

4.9. Verification against the relation Pore-Pressure – Deformation at the borehole

4.9.1. Elastic behaviour (virgin loading, for p<1050kPa and cycles)

For elastic loading (Figure 13) the theoretical curve (uw Teo, Blue triangle) is well represented compared to the experimental curve (uw Exp, Green circle), including
cycles. It should be noted that over the three cycles carried out, the pore pressure varies with the same differences than the total pressure.

4.9.2. Plastic behaviour (virgin loading, p>1050kPa)

In the plastic field, the calculation is made with a cohesion and friction angle according to the previous equations- The experimental behaviour is not typical of a coherent soil, but rather that to a frictional soil with an angle Φ of 22° (with a cohesion of 37kPa, with a contractancy of -3.7°).

It can be seen that the experimental slope of the relationship (**Figure 4**) Log(p'+c'/Tg(Φ'))-Log(ε_θ) is equal to the experimental slope, and that the theoretical curve (**Figure 13**) covers pretty well the experimental one.

5. Discussion

We performed the interpretation of the pressuremeter test in Undrained, almost Saturated conditions with an elasto-plastic soil in nonlinear elasticity, neglecting soil consolidation and creep.

<u>In elastic state</u>, we showed:

• In the case of non-linear elastic soil, there is an increase in pore pressure during pressure shearing; this increase in pore pressure is related to the decrease of the soil shear modulus function of ε_θ.

• The total orthoradial stress is not symmetrical of the total radial stress with respect to p_0,

• Only the effective orthoradial stress is symmetric of the effective radial stress from p'_0

• The pore pressure varies linearly as a function of the total pressure with a known coefficient, B_{pres}

• The Undrained shear modulus is consistently stronger than the Drained shear modulus-(in a ratio of 20 at virgin loading, and 5 at cyclic)

<u>In plastic state</u> :

• Creep pressure is indicated by the slope break between pore pressure and total pressure

• The pore pressure varies linearly as a function of the total pressure with a theoretically known coefficient, in elasticity B^P_{pres}•

•The pore pressure varies linearly as a function of the plastic deformation, which allows us to determine the contractancy Ψ (with our measurements) or the dilatancy,

• The effective creep pressure is used to determine the pair value (c', Φ '),

• The linear Log-Log relationship between the effective stress and the deformation at the borehole strain is used to determine the pair value (c', Φ'),

• The average value of the pair value (c', Φ ') is used to calculate a theoretical pressuremeter curve in agreement with the experimental one with two relationships (p - ε_θ) and (u_{w-} ε_θ)

The areas for improvement should be :

• taking into account the time phenomenon during the test, which will change or suppress the constant Cγ

Taking into account the actual area of influence of the pressuremeter (should be 6 time its radius) on the increase of the pore pressure, and not assume an infinite influence of the loading along the radius.

6. Conclusions and outlook

This research showed the importance of taking into account the hydromechanical coupling in the interpretation of the pressuremeter. The actual parameters used in the numerical models are very different from those estimated in total stress in the pressuremeter test for fine soils in an undrained situation. In addition, the response of the soil under total stress is very far from the behaviour of an elasto-plastic soil. Thus, the use of apparent parameters that do not explicitly take into account pore pressure seems to be an unsuitable approach .

For the calculation of moduli, the shear moduli calculated with the total stresses are 5 to 20 times greater than calculated with effective stress.

To properly calibrate the models, we recommend special pressuremeter tests including:

- Measurement of pore pressure during the test;
- 3 unload/reloading cycles;

This type of test, with an in-depth interpretation, allows calibrating a large part of the parameters necessary for the behaviour laws used in elaborate numerical models (HSM laws, HSM Small)

Additional research actions will be undertaken to test this new method of analysis on other pressuremeter tests in different depths and soils.

7. Other notations

a : radius of the borehole
b : plastic radius
β : slope of the relation u_w ε_θ in plasticity
B_{pres}^{p} : Skempton coefficient for pressuremeter
ε_r : radial strain
ε_θ : orthoradial strain
G_s : secant shear modulus in Total stress
G'_s : secant shear modulus in Effective stress
G_t : tangent shear modulus in Total stress
G'_t : tangent shear modulus in Effective stress
G'_{tsu} : tangent shear modulus in Effective stress for large deformation
G'_{sB} : secant shear modulus at the plastic radius b in Effective stress
n : porosity of the soil
N_f : Failure ratio eq. (12)
n_e : Dilatancy ratio eq. (13)
p : Total pressure applied at the borehole wall
p' : Effective pressure applied at the borehole
r : radius
s : suction
R_i : radius at level i
S : surface of the soil between R_i and R_{i-1}
s_{air} : suction at the air entry
S_r : degree of saturation
$S_{r\text{-}air}$: degree of saturation at the air entry
S_{re} : degree of saturation for un null suction
$S_{r\text{-}res}$: residual saturation degree when the water is fully adsorbed
σ_r : Total radius stress
σ'_r : Effective radius stress
σ_θ : Total orthoradial stress
σ'_θ : Effective orthoradial stress
u_w : pore pressure of the mixture air-water

8. References

Arulrajah, A., Bo, M.W., and Piratheep, J. 2011. In Situ Testing of Soft Soil at a Case Study Site with the Self-Boring Pressuremeter. Geotechnical Testing Journal,.

Baguelin, F., Jezequel, J.F., and Shields, D.H. 1978. The pressuremeter and foundation engineering,. Trans Tech Publications, Aedermannsdorf, Switzerland.

Boutonnier, L. 2007, October 23. Comportement hydromécanique des sols fins proches de la saturation. Thèse INPG Grenoble.

Cao, L.F., Teh, C.I., and Chang, M.F. 2001. Undrained cavity expansion in modified Cam clay I: Theoretical analysis. Géotechnique, **51**: 323–334.

Carter, J.P., Randolf, M.F., and Wroth, C.P. 1979. Stress and pore pressure changes in clay during and after the expansion of a cylindrical cavity. Int. J. for Num. Anal. Met. in Geom.: 305–322.

Duncan, J.M., and Chang, C.Y. 1970. Non linear analysis of stress and strain in soils. Journal of Soil Mechanics and Foundation Division, SM 5: 1629–1653.

Gibson, R.E., and Anderson, W.F. 1961, May. In-Situ measurement of Soil Properties with the pressuremeter. Civil Rng. and Public Works Review,: 615–618.

Habert, J., and Burlon, S. 2020. Taking into account inhomogeneous distortion around the pressuremeter probe to determine shear modulus. In ISC6. Budapest.

Hughes, J., and Whittle, R.W. 2023. High resolution pressuremeters - the measurement of small things. CRC Press - Taylor & Francis Group, Boca Raton.

Monnet, J. 2012. Elasto-plastic analysis of the pressuremeter test in granular soil – part I: theory: European Journal of Env. and Civil Engineering, 16: 699–714.

Monnet, J., Boutonnier, L., and Mahmutovic, D. 2021. Elastic interpretation of unsaturated Undrained pressuremeter tests in clays. In 6th Int. Conf. on Geotech. p. p1.-7.

Monnet, J., and Chemaa, T. 1994. Etude théorique et expérimentale de l'équilibre élasto-plastique d'un sol cohérent autour du pressiomètre. Revue Française de Géotechnique,: 15–26.

Plaxis corp. 2021. Plaxis Version 8 - Material Models Manual. Available from https://communities.bentley.com

Santos, J.A., and Correia, A.G. 2001. Reference threshold shear strain of soil. Its application to obtain a unique strain-dependant shear modulus curve for soil. SMGE. Istanbul. pp. 267–270.

Silvestri, V., and Abou-Samra, G. 2012. Analytical solution for undrained plane strain expansion of a cylindrical cavity in modified Cam Clay. Geomechanics and Engineering,: 19–37.

Skempton, A.W. 1954. The Pore-Pressure Coefficients A and B | Géotechnique. Géotechnique, 4: 143–147.

Wroth, C.P., and Windle, D. 1977, September. Use of Self boring pressuremeter to determine the ubdrained properties of clay. Ground Engineering,: 37–45.